physica status solidi

pss

www.pss-journals.com

reprint

WILEY-VCH

Phys. Status Solidi A **209**, No. 12, 2514–2520 (2012) / **DOI** 10.1002/pssa.201228305

physica status solidi a
www.pss-a.com
applications and materials science

Effects of surface modification of carbon nanotube on platinum nanoparticle deposition using supercritical carbon dioxide fluid

Mitsuhiro Watanabe*, **Tatsunori Akimoto, and Eiichi Kondoh**

Interdisciplinary Graduate School of Medicine and Engineering, University of Yamanashi, 4-3-11 Takeda, Kofu, Yamanashi 400-8511, Japan

Received 14 May 2012, accepted 22 August 2012
Published online 21 September 2012

Keywords carbon nanotube, plasma treatment, platinum nanoparticle, supercritical carbon dioxide fluid

* Corresponding author: e-mail mitsuhirow@yamanashi.ac.jp, Phone: +81 55 220 8473, Fax: +81 55 220 8473

Platinum nanoparticles were fabricated on multiwalled carbon nanotubes (MWCNTs) by using supercritical fluid deposition. In this technique, deposition was carried out in a supercritical carbon dioxide fluid via hydrogen reduction of a dissolved platinum complex. The deposition temperature and deposition-time dependences on the particle size and density were investigated. The obtained metallic nanoparticles/MWCNT nanocomposites were characterized by using transmission electron microscopy and scanning transmission electron microscopy. Crystalline pure platinum nanoparticles were clearly observed on the surfaces of MWCNTs. Most of the particles observed were smaller than 5 nm in diameter. The density of the particles increased with temperature between 393 and 423 K and decreased above 423 K. The nucleation of the nanoparticles took place within a deposition time of 60 min, and then agglomeration and coarsening occurred, resulting in an increase of the particle size. It was found that the surface topography of the carbon support greatly influences the platinum nucleation density. Indeed, when the MWCNTs were treated with hydrogen plasma prior to platinum deposition, the density of the nanoparticles markedly increased. The impact of the hydrogen plasma treatment on the particle-size dependences was also investigated.

1 Introduction Synthesis and processing of nanomaterials in supercritical fluids, especially in supercritical carbon dioxide ($scCO_2$) fluid, have been attracting extensive attention in recent years. The supercritical fluid is a state that exists above the critical point of a material (CO_2: 7.38 MPa, 304.2 K [1]) and has many unique properties, such as zero surface tension, low viscosity, and excellent diffusivity like a gas phase, and high density and solvent capability like a liquid phase. These characteristics make the $scCO_2$ fluid a promising transport medium for delivering reactant molecules to features having nanosized complicated surfaces and/or poorly wettable surfaces.

Supported metal nanoparticles have unique electronic, optical, and catalytic properties [2]. These properties are directly related to their size and distribution. Commonly used catalysts in fuel cells are nanoparticles of precious metals, such as platinum and platinum-based alloys, which are deposited on conductive supports. Carbon black has been most widely used as a support for fuel-cell catalysts because it possesses both electronic conductivity and extremely large surface area [3, 4]. Recently, carbon nanotubes (CNTs) have attracted special attention due to their overwhelming catalytic and electronic properties versus carbon black. Several techniques for preparing CNT-supported platinum nanoparticles have been attempted so far, such as electrodeposition [5–8], electroless deposition [9], hydrothermal synthesis [10], microwave heating [11–13], and microemulsion synthesis [14]. However, these conventional preparation techniques do not always provide adequate nanoscale controllability of the particle shape and size. Therefore, the synthesis of nanoparticles on the CNT still remains as a challenge in terms of obtaining the desirable size dispersion for electrocatalytic uses.

The synthesis of platinum nanoparticles/carbon nanocomposites using supercritical fluids, usually $scCO_2$ fluid, has been reported as an alternative technique [15–19], where the formation of nanoparticles down to several nanometers in diameter was the main concern. In order to obtain such a small particle size with a narrow dispersion reproducibly, it is important to understand the dependences of the particle size on deposition conditions in detail.

In the present study, platinum nanoparticles were deposited on plasma-modified and unmodified CNTs in $scCO_2$ fluid under various deposition temperature and time conditions. The size and dispersion of the nanoparticles were investigated, and nucleation and growth behaviors on CNT surfaces were discussed.

2 Experimental procedure Multiwalled carbon nanotubes (MWCNTs) were used as a support. The surface modification of MWCNTs was performed in hydrogen plasma. The MWCNTs were placed in a glass tube, and this tube was filled with gaseous hydrogen to 0.3 MPa after evacuation. Then, an electrodeless microwave (2.45 GHz) discharge was generated around the specimen, by using a microwave cavity, at a plasma power density of approximately 10 W cm^{-3}. The working pressure and treatment time were fixed at 130 Pa and 5 min, respectively.

A schematic illustration of the deposition apparatus is shown in Fig. 1. The deposition conditions are summarized in Table 1. In the present study, a batch-type reaction system was used [20]. The precursor used was bis(hexafluoroacetylacetonate)-platinum(II) ($Pt(C_5HF_6O_2)_2$, hereafter $Pt(hfac)_2$). The precursor and the support were weighed to 1.0 and 0.5 mg, respectively, and were placed at the bottom of a pressure-resistant steel cell (2.1×10^{-3} dm^3). After filling the cell with gaseous hydrogen to 1 MPa, pressurized liquid CO_2 was added to the cell with a high-pressure pump for liquid chromatography. The cell was heated to a target temperature with a heating mantle and the temperature was held for a scheduled duration (deposition time), followed by depressurization and cooling. Deposition was carried out at different deposition temperatures and times (393 to 473 K, 30 to 90 min). The morphology and size of nanoparticles were characterized with transmission electron microscopes (TEMs) (JEOL 2000FX-II and FEI Tecnai Osiris) and a Hitachi HD 2300C scanning transmission electron microscope (STEM). Chemical composition analyses were carried out by using an energy-dispersive X-ray (EDX) spectrometer equipped to the STEM. Copper grids were used for TEM and STEM observations, where the MWCNT-supported nanoparticles were lifted on the grid by using ultrasonic suspension in ethanol.

Table 1 Deposition conditions.

deposition temperature (K)	393–473
deposition time (min)	30–90
hydrogen partial pressure (MPa)	0.7
total pressure (MPa)	10

3 Results

3.1 Characterization of platinum nanoparticle/MWCNT nanocomposites synthesized in $scCO_2$ fluid Figure 2a shows a bright-field image of MWCNT-supported nanoparticles deposited in $scCO_2$ fluid. Isolated nanoparticles were clearly observed on the surfaces of the MWCNT. These deposited nanoparticles seemed to align on concave lines present at the MWCNT surfaces. The nanoparticles were observed in a circular shape in any of the observation directions, indicating that the nanoparticles were spherical. Most of the nanoparticles were smaller than 5 nm in diameter. Figure 2b shows a bright-field image of nanoparticles formed on plasma-treated (PTed) MWCNTs under the deposition condition as in Fig. 2a. As well as in the case of the non-treated (NTed) MWCNT (Fig. 2a), the nanoparticles had a diameter smaller than 5 nm.

Figure 3 shows a typical Z-contrast image of a nanoparticle/MWCNT nanocomposite. The nanoparticles have a stronger image contrast than MWCNT, obviously indicating that the nanoparticles were composed of a much heavier element than carbon. Figure 4 shows a high-resolution TEM image of a deposited nanoparticle. Lattice planes were clearly observed. The determined lattice spacing

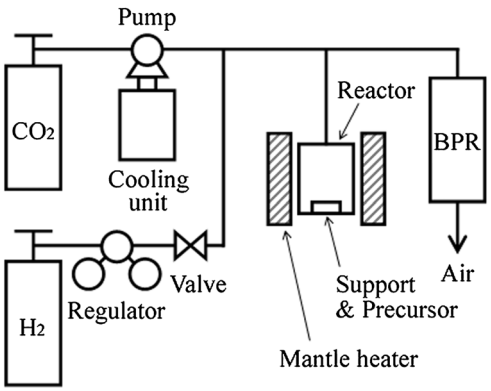

Figure 1 Schematic diagram of $scCO_2$ fluid deposition apparatus.

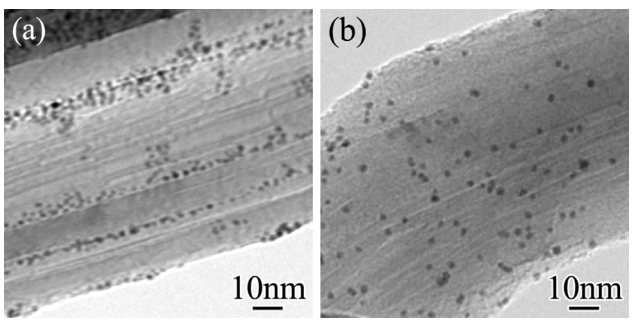

Figure 2 Bright-field images of nanoparticles supported on (a) non-treated (NTed) and (b) plasma-treated (PTed) MWCNT.

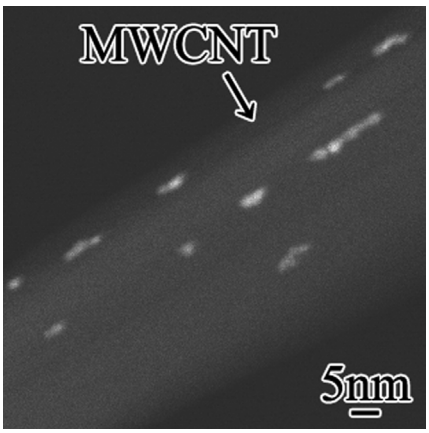

Figure 3 A typical Z-contrast image of nanoparticle/MWCNT nanocomposite.

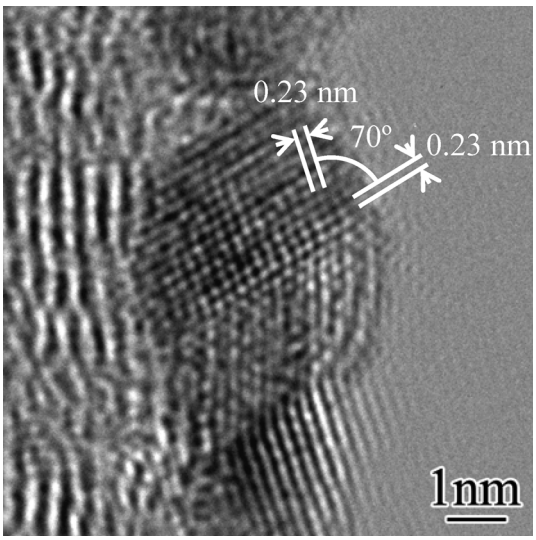

Figure 4 High-resolution TEM image of a nanoparticle deposited on MWCNT surface.

corresponded to that of {111} of platinum. These analyses revealed that the nanoparticles deposited on the MWCNTs were crystalline pure platinum.

3.2 Temperature dependence of nanoparticle size Figure 5 shows the temperature dependence of the size distributions of the platinum nanoparticles grown on NTed and PTed MWCNTs. Inset shows the detailed size distribution of platinum nanoparticles smaller than 5 nm in diameter. Solid and open bars correspond to NTed and PTed MWCNTs, respectively. Regardless of the presence/absence of the plasma treatment, nanoparticles smaller than 5 nm were deposited on the MWCNT surfaces at temperatures between 393 and 473 K. The density of nanoparticles smaller than 5 nm increased with increasing temperature but decreased above 423 K. The density peak position shifted to the right with increasing temperature, indicating that particle coarsening took place. Table 2 shows the mean diameter, the total volume, and the density of the platinum nanoparticles. The mean diameter, approximately 2.5 nm, hardly depended on deposition temperature. The volume of the platinum nanoparticles decreased with increasing deposition temperature.

When the PTed MWCNTs were used, the density of the platinum nanoparticles increased more than when the NTed MWCNTs was used. This tendency was remarkable for much smaller particles (<2 nm) and was observed in all temperature ranges, whereas the density of relatively coarse particles (>5 nm) was almost unchanged (Fig. 5). The temperature dependences of the size distribution, the mean diameter, the total volume, and the density of the platinum nanoparticles for the PTed MWCNTs were similar to those for the NTed MWCNTs, as shown in Fig. 5 and Table 2.

3.3 Deposition-time dependence of nanoparticle size Figure 6 shows the deposition-time dependence of the size distributions of the platinum nanoparticles grown on NTed and PTed MWCNTs. The mean diameter, the total volume, and the density are shown in Table 3. Regardless of performing the plasma treatment, the mean diameter of the nanoparticles increased with increasing deposition time. When the deposition time was 30 min, all observed nanoparticles were smaller than 5 nm in diameter. The particle density increased when a longer deposition time of 60 min was used. Though most of the nanoparticles deposited were smaller than 5 nm, nanoparticles larger than 5 nm were also observed. However, at a deposition time of 90 min, particles larger than 5 nm became dominant and nanoparticles smaller than 5 nm decreased drastically in number. The density peak position shifted to the right with increasing deposition time, indicating that particle coarsening occurred.

When the PTed MWCNTs were used, the density peak position shifted to the left and nanoparticles smaller than 5 nm increased more markedly than when the NTed MWCNTs was used. This tendency was observed for all the deposition times. The deposition-time dependences of the size distribution, the mean diameter, the total volume, and the density of the platinum nanoparticles for the PTed MWCNTs were similar to those for the NTed MWCNTs, as shown in Fig. 6 and Table 3.

4 Discussion In this section, we first discuss a general tendency of the nucleation and growth of platinum nanoparticles on MWCNTs (Section 4.1). On this basis, the effects of plasma treatment will be discussed next (Section 4.2).

4.1 Nucleation and growth of platinum nanoparticle on MWCNT Most of the nanoparticles deposited on MWCNTs had a diameter smaller than 5 nm at any temperatures employed in the present study. The density increased with increasing temperature up to 423 K but decreased above 423 K. When the deposition time was

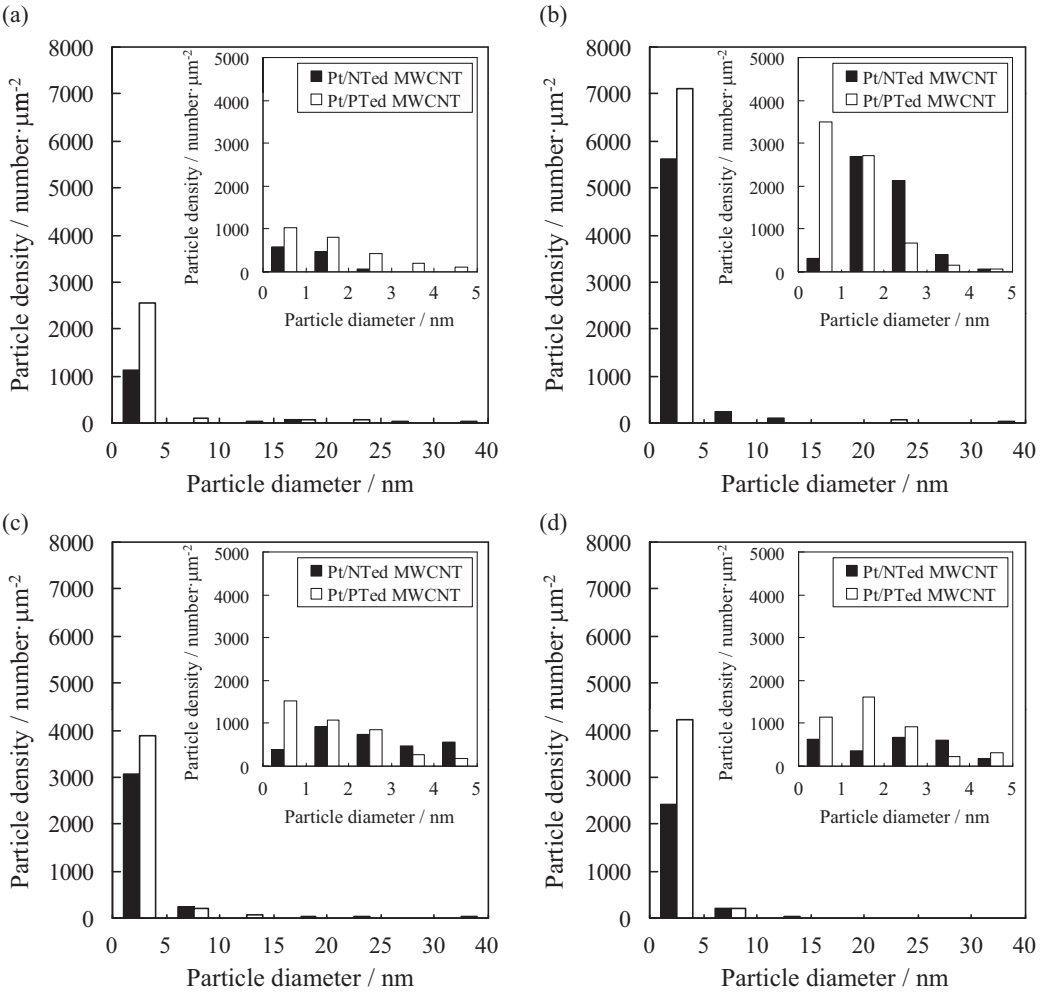

Figure 5 Size distributions of platinum particles grown on NTed and PTed MWCNTs. Deposition temperatures were (a) 393 K, (b) 423 K, (c) 453 K, and (d) 473 K, respectively.

increased, the particle density increased up to 60 min but decreased for longer deposition times. The mean diameter of the nanoparticles also increased with increasing deposition time.

The rate of the deposition reaction is generally proportional to both precursor concentration and deposition temperature. Therefore, the total volume of nanoparticles is expected to increase with increasing deposition temperature. In the previous study, when activated carbon (Ketjenblack (KB)) was used, we observed an increment of the total volume of the platinum nanoparticles with increasing deposition temperature [21]. However, in the present study, we observed that the volume of the nanoparticles decreased with increasing deposition temperature. This indicates that

Table 2 Temperature dependence of total platinum nanoparticles for NTed and PTed MWCNTs.

temperature (K)	mean diameter (nm)		volume ($\times 10^5$ nm^3 μm^{-2})		particle density ($\times 10^3$ μm^{-2})	
	NTed	PTed	NTed	PTed	NTed	PTed
393	2.8	2.6	6.4	9.8	1.2	2.8
423	2.4	1.3	1.9	5.1	6.0	7.2
453	2.7	2.2	0.78	4.1	3.3	4.2
473	2.4	2.1	0.49	1.2	2.6	4.5

NTed, non-treated MWCNT; PTed, plasma-treated MWCNT.

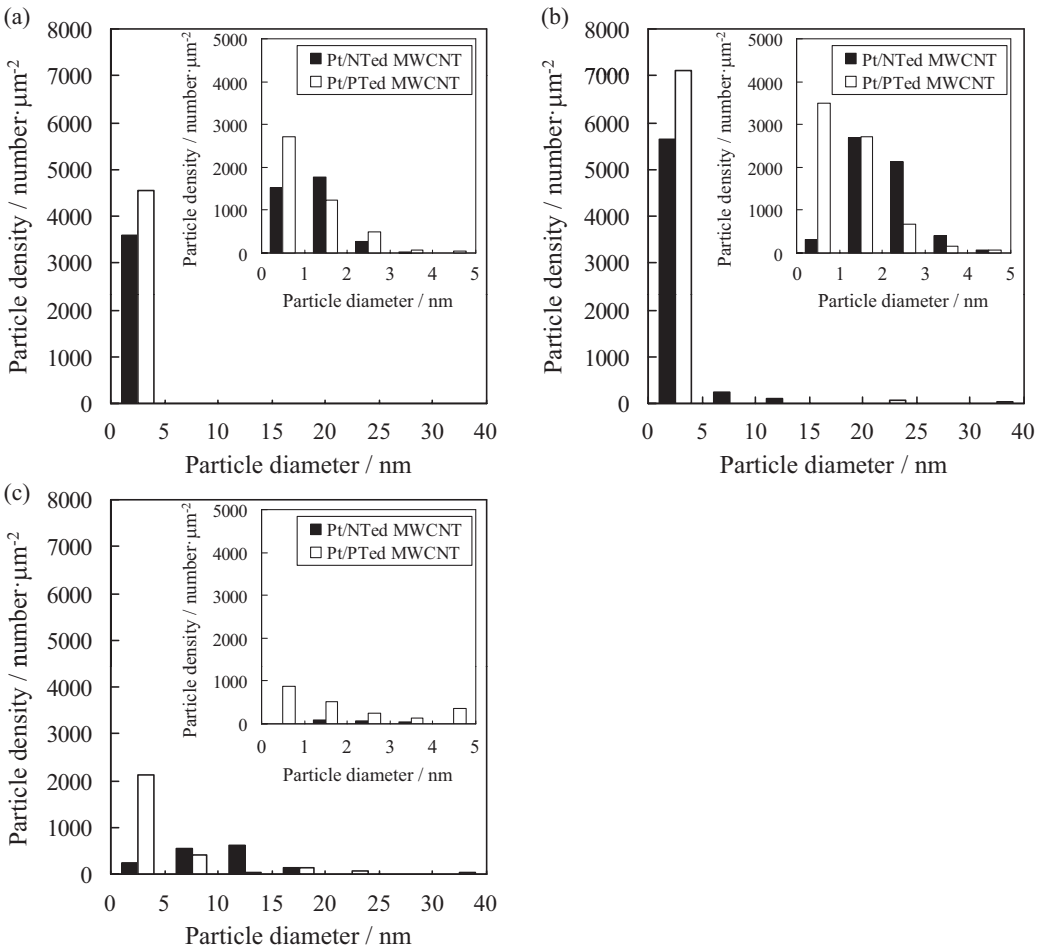

Figure 6 Size distributions of platinum particles grown on NTed and PTed MWCNTs. Deposition times were (a) 30 min, (b) 60 min, and (c) 90 min, respectively.

the nucleation of the nanoparticle is difficult on MWCNTs. It is expected that the nucleation concentrates and then the precursors adsorb preferentially to the nuclei and growth of the particle occurs at a specific part at a lower temperature. As a result, coarse particles were produced and relatively high volume was obtained in the observation range. The MWCNT surface is activated with increasing deposition temperature and the nucleation area expands. Consequently, finer particles were extensively generated because the precursor consumption takes place homogeneously over a broad range of areas on MWCNTs. Therefore, in the present study, the decrement of the volume of the platinum nanoparticles with increasing deposition temperature was observed.

At a low temperature (393 K), a lower particle density was observed, as shown in Fig. 5 and Table 2. As mentioned above, the reaction rate of the precursor decomposition decreased with decreasing temperature. Therefore, lowering of the particle density, or lowering of the density of the nucleation site is considered to be due to the lowering of the

Table 3 Deposition-time dependence of total platinum nanoparticles for NTed and PTed MWCNTs.

time (min)	mean diameter (nm)		volume ($\times 10^5$ nm^3 μm^{-2})		particle density ($\times 10^3$ μm^{-2})	
	NTed	PTed	NTed	PTed	NTed	PTed
30	1.1	1.0	0.056	0.96	3.6	4.6
60	2.4	1.3	1.9	5.1	6.0	7.2
90	9.6	3.6	10	9.9	1.5	2.8

NTed, non-treated MWCNT; PTed, plasma-treated MWCNT.

reaction rate, which was observed at 393 K. This agrees with our other results that the particle density increased with temperature between 393 and 423 K. However, when the temperature was above 423 K, the particle density decreased and the mean particle diameter increased with increasing deposition temperature. This indicates that another phenomenon become dominant. We presume that the platinum atoms detached from relatively unstable fine particles and absorbed onto relatively stable coarse particles; i.e. the Ostwald ripening took place. As a result, the particle density decreased and the mean particle diameter increased at higher temperatures.

When the deposition time was short (30 min), the particle density was lower, or the nucleation density was lower, as shown in Fig. 6 and Table 3. When the deposition time was intermediate (60 min), the density of the nanoparticles was increased by an increase of nucleation density, thus by an increase of reaction time, as expected. However, when the deposition time was longer than 60 min, we observed a decrease of the particle density. This indicates that the nucleation of the nanoparticles almost completed within 60 min. After this time, the density of the nanoparticles smaller than 5 nm decreased drastically and the density of the nanoparticles larger than 5 nm increased. Also, the mean particle diameter increased accompanying a decrease of particle density. This indicates that the Ostwald ripening mechanism influenced the growth of the nanoparticles.

The above-mentioned particle density tendencies were basically similar to our previous study on KB [21]. One significant difference is that the density of the nanoparticles deposited on KB was much higher (e.g. $9.5 \times 10^3\ \mu m^{-3}$ at 423 K, 60 min) than that on MWCNT (e.g. $6.0 \times 10^3\ \mu m^{-3}$ at 423 K, 60 min). We assume that this is due to higher surface roughness of the KB than the MWCNT. As shown in Fig. 2a, the nanoparticles were deposited preferentially at the concave parts of the MWCNT surface. The density of the nucleation sites increases with increasing surface roughness; and therefore, it should be effective to roughen the carbon support surface for the deposition of a high density of nanoparticles.

4.2 Effects of plasma treatment of MWCNTs on platinum nanoparticle deposition Now, we look the results on the formation of platinum nanoparticles deposited on the PTed MWCNTs, for instance, Fig. 2b. Obviously, the density of the nanoparticles increased on the PTed MWCNTs than that on the NTed MWCNTs at all the temperatures and deposition times. The results are summarized in Tables 2 and 3.

Plasma irradiation is known to introduce defects at materials surfaces [22, 23]. Zhang et al. [24] and Gohel et al. [25] investigated the field emission properties of plasma-irradiated CNTs. They indicated that the defects were introduced at the surface of CNTs by plasma irradiation so that the density of the field emission sites increased drastically. These studies evidenced that the plasma irradiation introduces defects and roughening of the CNT surfaces.

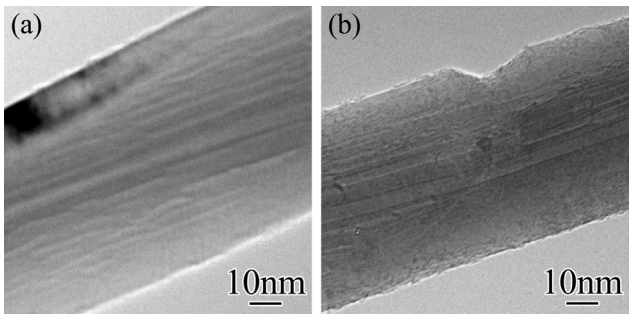

Figure 7 Bright-field images of MWCNT surface (a) before and (b) after plasma treatment.

Figure 7 shows bright-field images of the MWCNT surface before and after the plasma treatment. The PTed MWCNT was obviously rougher, which agrees reasonably with previous works cited above. As mentioned in Section 4.1, the nucleation of nanoparticles occurs preferentially at the locations having larger surface roughness. From these reasons, we now conclude that the particle density increased on the PTed MWCNTs because the nucleation sites of the platinum nanoparticles increased.

5 Conclusions The platinum nanoparticles were deposited on the NTed and PTed MWCNTs in supercritical CO_2 fluid with different deposition temperatures and deposition times. The following findings were obtained:

Crystalline pure platinum nanoparticles were grown on the MWCNTs. Most of the nanoparticles had a diameter <5 nm.

The density of the nanoparticles increased with increasing temperature up to 423 K and decreased above 423 K. Also, the density of the nanoparticles increased with increasing deposition time up to 60 min and then decreased for longer deposition times. These tendencies indicate that the nucleation of the nanoparticles took place mainly at a lower temperature and/or at an earlier deposition time, and agglomeration and coarsening become dominant at a higher temperature and/or at a later deposition time.

The density of the platinum nanoparticles increased when the MWCNTs were pretreated with hydrogen plasma. This was found to be effective in roughening the carbon support to achieve the deposition of a high density of nanoparticles.

References

[1] R. Span and W. Wagner, J. Phys. Chem. **25**, 1509 (1996).
[2] K. S. Morley, P. C. Marr, P. B. Webb, A. R. Berry, F. J. Allison, G. Moldovan, P. D. Brown, and S. M. Howdle, J. Mater. Chem. **12**, 1898 (2002).
[3] J. T. Moore, J. D. Corn, D. Chu, R. Jiang, D. L. Boxall, E. A. Kenik, and C. M. K. Lukehart, Chem. Mater. **15**, 3320 (2003).
[4] W. H. Lizcano-Valbuena, D. C. Azevedo, and E. R. Gonzalez, Electrochim. Acta **49**, 1289 (2004).
[5] M. C. Tsai, T. K. Yeh, and C. H. Tsai, Electrochem. Commun. **8**, 1445 (2006).

[6] G. G. Wildgoose, C. E. Banks, and R. G. Compton, Small **2**, 182 (2006).
[7] Y. Zhao, L. Fan, H. Zhong, and Y. Li, Microchim. Acta **158**, 327 (2007).
[8] Y. Zhao, L. Fan, H. Zhong, Y. Li, and S. Yang, Adv. Funct. Mater. **17**, 1537 (2007).
[9] G. Guo, F. Qin, D. Yang, C. Wang, H. Xu, and S. Yang, Chem. Mater. **20**, 2291 (2008).
[10] L. Chen and G. Lu, Electrochim. Acta **53**, 4316 (2008).
[11] J. Zhao, P. Wang, W. Chen, R. Liu, X. Li, and Q. Nie, J. Power Sources **160**, 563 (2006).
[12] C. M. Chen, M. Chen, H. W. Yu, S. C. Lu, and C. F. Chen, Jpn. J. Appl. Phys. **47**, 2324 (2008).
[13] S. Wang, S. P. Jiang, T. J. White, J. Guo, and X. Wang, J. Phys. Chem. **113**, 18935 (2009).
[14] K. Shimizu, I. F. Cheng, J. S. Wang, C. H. Yen, B. Yoon, and C. M. Wai, Energy Fuels **22**, 2543 (2008).
[15] Y. Lin, X. Cui, C. Yen, and C. M. Wai, J. Phys. Chem. B **109**, 14410 (2005).
[16] A. D. Taylor, R. C. Sekol, J. M. Kizuka, S. D'Cunha, and C. M. Comisar, J. Catal. **259**, 5 (2008).
[17] T. Machino, W. Takeuchi, H. Kano, M. Hiramatsu, and M. Hori, Appl. Phys. Express **2**, 025001 (2009).
[18] E. E. Said-Galiyev, A. Y. Nikolaev, E. E. Levin, E. K. Lavrentyeva, M. O. Gallyamov, S. N. Polyakov, G. A. Tsirlina, O. A. Petrii, and A. R. Khokhlov, J. Solid State Electrochem. **15**, 623 (2011).
[19] K. Mase, H. Kondo, S. Kondo, M. Hori, M. Hiramatsu, and H. Kano, Appl. Phys. Lett. **98**, 193108 (2011).
[20] E. Kondoh, K. Sasaki, and Y. Nabetani, Appl. Phys. Express **1**, 061201 (2008).
[21] T. Akimoto, M. Watanabe, and E. Kondoh, J. Surf. Finish. Soc. Jpn. **63**, 365 (2012).
[22] Y. Yamazaki, K. Ishikawa, S. Samukawa, and S. Yamazaki, Phys. B **376/377**, 327 (2006).
[23] K. Eriguchi, A. Ohno, D. Hamada, M. Kamei, and K. Ono, Thin Solid Films **516**, 6604 (2008).
[24] J. Zhang, T. Feng, W. Yu, X. Liu, X. Wang, and Q. Li, Diam. Relat. Mater. **13**, 54 (2004).
[25] A. Gohel, K. C. Chin, Y. W. Zhu, C. H. Sow, and A. T. S. Wee, Carbon **43**, 2530 (2005).

